Light-powered reactivation of flagella: towards building an artificial cell

R. Ahmad[1†], C. Kleineberg[2†], V. Nasirimarekani[3], Y. Su[1], S. Goli Pozveh[1], A. J. Bae[1‡], E. Bodenschatz[1,4], K. Sundmacher[2,5], I. Guido[1], T. Vidaković-Koch[2*], A. Gholami[1*]

[1]Max Planck Institute for Dynamics and Self-Organization, Am Fassberg 17, 37077 Göttingen, Germany
[2]Max-Planck Institute for Dynamics of Complex Technical Systems, Sandtorstraße 1, 39106 Magdeburg, Germany
[3]Microfluidics & BIOMICS Cluster UPV/EHU, University of the Basque Country UPV/EHU, 01006, Vitoria-Gasteiz, Spain
[4]Institute for Dynamics of Complex Systems, Georg-August-University Göttingen, 37073 Göttingen, Germany
[5]Otto von Guericke University, Universitätsplatz 2, 39106 Magdeburg, Germany

***For correspondence:** azam.gholami@ds.mpg.de; vidakovic@mpi-magdeburg.mpg.de
[†]These authors contributed equally to this work.
[‡]**Present address:** Department of Biomedical Engineering, University of Rochester, USA.

Abstract

Artificial systems capable of self-sustained movement with self-sufficient energy are of high interest with respect to development of many challenging applications including medical treatments but also technical applications. The bottom-up assembly of such systems in the context of synthetic biology is still a challenging task. Here, we demonstrate the biocompatibility and efficiency of an artificial light-driven energy module and a motility functional unit by integrating light-switchable photosynthetic vesicles with demembranated flagella, thereby supplying ATP for dynein molecular motors upon illumination. Flagellar propulsion is coupled to its beating frequency and light-driven dynamic synthesis of ATP enabled us to control beating frequency of flagella as a function of illumination. Our integrated system has potential biomedical applications in the subject of targeted drug delivery. Further, we verified the functionality of light-powered synthetic vesicles in *in vitro* motility assays by encapsulation of microtubules assembled with force-generating kinesin-1 motors and energy module to investigate dynamics of a contractile filamentous network by optical stimulation. Integration of our photosynthetic system with different biological building blocks such as cytoskeletal filaments and molecular motors may contribute to the bottom-up synthesis of artificial cells that are able to undergo motor-driven morphological deformations and exhibit directional motion in a light-controllable fashion.

1 Introduction

Bottom-up synthetic biology is an emerging field of science focusing on engineering of life-like structures. These artificial constructs mimic some of the essential life processes like reproduction, growth, motility, etc. Reconstitution of each of these processes is quite complex, so the bottom-up synthetic biology focuses at

first to sub-systems (functional modules), which are hand-tailored to partially or entirely mimic some of essential life processes (1–3). Later on these functional modules can be combined to build up higher hierarchical structures. With this respect, artificial systems capable of moving forward are highly attractive for different applications. Examples are smart drug delivery vehicles, or so-called designer immune cells which would be capable of detecting and moving towards a chemical signal or tumor (4). In these applications motility is only one of functionalities, but even its reconstitution is quite challenging since it embraces, not only the assembly of molecular motors (a motility functional module) which enable movement but also the delivery of energy-rich ATP molecules (energy functional module).

In nature different motility mechanisms are evolved, including polarized assembly and disassembly of bio-polymers for directional motion of amoboid cells (5, 6), or propulsion powered by ancient organelles cilia and flagella which perform whip-like motion (7) to provide motility for primitive eukaryotic cells living in an aqueous environment (8). Cilia and flagella are composed of a microtubule-based structure called axoneme which is covered by a plasma membrane (9, 10). Nine microtubule doublets, each formed of a complete A-microtubule and an incomplete B-microtubule, are cylindrically arranged around two microtubule singlets in the middle. The diameter of an axoneme is around 200 nm, and the adjacent microtubule doublets are spaced 30 nm away from each other (11). The functionality and structural properties of cilia and flagella are the same and can be classified as motile (9+2) and immotile sensory (9+0) cilia. To date, more than 250 constituent proteins have been found to contribute to the highly ordered and precisely assembled structure of axoneme (12). The microtubule doublets and the dynein molecular motors are the most important components of axonemes (13, 14). Axonemal dyneins are highly specific for ATP as substrate (15, 16). In the presence of ATP, dynein molecular motors, which are statically bound to the A tubules of each doublet, attach themselves transiently to the B tubules of teh neighboring doublet and generate internal stresses to displace adjacent microtubules relative to each other. However, since microtubule doublets are mechanically connected to the neighboring doublets and cannot slide freely (17), this sliding force is converted into a bending motion. The bottom-up reconstitution of flagella is of significant complexity, thereby we isolated this functional module from green algae *Chlamydomonas reinhardtii*. The isolated motility functional module has all infrastructure required for a directed movement, but ATP fuel is lacking. Therefore an ATP regeneration module is required for a self-sustained motility. Furthermore, microtubules are one of the cytoskletal filaments which together with actin and intermediate filaments provide shape and motility in eukaryotic cells and play very important role in various cellular processes (18, 19). Encapsulation of MTs and other cytoskeletal filaments (20) to build an energetically autonomous artificial cell is a challenging task in the field of synthetic biology and again highlights the necessity of a self-sufficient energy production system.

With respect to this, we recently reviewed (1) different strategies for ATP regeneration in the context of bottom-up synthetic biology and we reported on different types of energy functional modules (21, 22). They are basically utilizing either chemical (21) or light energy (22) to regenerate ATP out of ADP. The later system appears especially promising for coupling with such bottom-up applications which rely only on ATP as an energy carrier and do

not involve NADH (NAD(P)H) reductive power, like in the case of motility. The light energy driven ATP regeneration is not novel; for mimicking natural photophosphorylation, a series of artificial systems have been constructed to capture the energy of light and move protons across the membranes (23). Simple prototypical systems, which combine light-driven proton pumps with the F_OF_1-ATP synthase in liposomes have been demonstrated already in the early 70s, the motivation being to develop *in vitro* models for the mechanistic understanding of F_OF_1-ATP synthase. By varying several different types of rhodopsins and F_OF_1-ATP synthases as well as of the lipid composition, the productivity of these assemblies was improved as shown by us (22) and other authors (24–27). Recently some examples showing coupling of light-driven ATP regeneration module with energy intensive tasks like CO_2 fixation (28) and actin contractions (29) as well as protein synthesis (30) were demonstrated. However, there was no study demonstrating self-sustained system showing directed movement driven by ATP.

In this contribution, we integrated a light-switchable bottom-up assembled ATP regeneration module with a motility functional unit which was isolated from green algae *Chlamydomonas reinhardtii*. Combination of these two modules leads to a dynamic synthesis of ATP and allows us to control beating frequency of flagella as a function of illumination. Our system has potential biomedical applications in the subject of smart drug delivery, as a flagellum attached to a drug-loaded vesicle can be propelled at various frequencies under varying illumination conditions. Additionally, to approach the ultimate goal of building an energetically independent artificial cell, we combined our photosynthetic vesicles with microtubule networks and molecular motors and subsequently encapsulated inside droplets. We observed controlled motor-driven contraction of filamentous network upon optical stimulation, indicating the efficiency of the artificial photosynthetic module in providing self-sufficient energy. Our integrated system has potential application in ATP-dependent motility assays, which aim to reconstitute motor-driven motion and force generation inside a synthetic cell, with the challenging goal of achieving light-controllable switch between motile and immotile state of an artificial cell.

2 Results

We engineered switchable photosynthetic liposomes (∼150 nm in diameter) as energy modules to generate ATP upon illumination. To convert light into energy, we co-reconstituted two purified transmembrane proteins namely, Bacteriorhodopsin (bR) and EF_OF_1-ATP synthase from E. coli. Upon illumination, Bacterorhodopsin pumps proton inside the vesicles interior, establishing a proton motive force that drives ATP synthase to catalyze the convertion of ADP to ATP (Fig. 1A). Both enzymes are isolated according to a standard procedure earlier described by Ishmukhametov, Galkin, and Vik (31) and Oesterhelt (32). Their purity is checked by SDS-PAGE analysis (SI, Fig. S1). bR is reconstituted in form of membrane patches to avoid material loss during solubilization. We recently showed that (22) the usage of monomeric, detergent-solubilized bR for reconstitution is also possible and will lead to functional ATP regeneration module. However, an almost uniform orientation of bR in PC liposomes could be only achieved when using bR in form of membrane patches (SI,

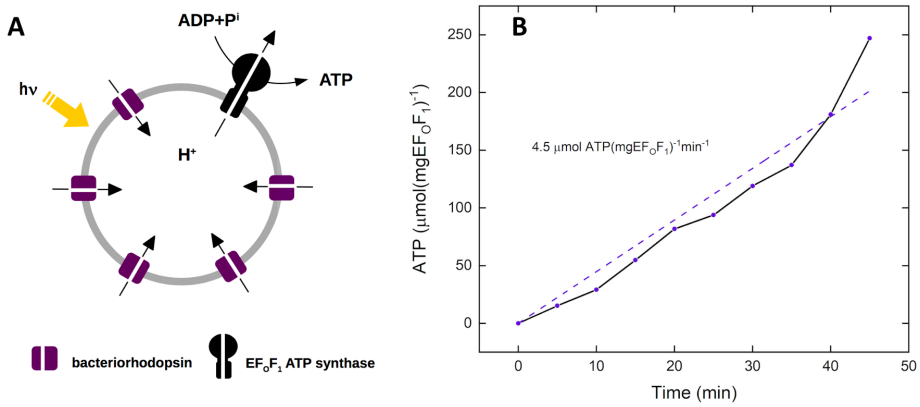

Fig. 1: Light-driven ATP production. A) Schematic representation of light-driven ATP synthesis in lipid vesicles. EF_OF_1-ATP synthase uses the electrochemical gradient generated by bacteriorhodopsin to synthesize ATP from ADP and Pi. B) Measurement of light-driven ATP production over time. The maximal rate of 4.5 µmol ATP $(mgEF_OF_1)^{-1}min^{-1}$ is determined by linear regression.

Fig. S2). Both enzymes are co-reconstituted into preformed phosphatidylcholine unilamellar vesicles using Triton X-100 as detergent, similar to the method described by Fischer and Gräber (33) for ATP synthase reconstitution. Liposomes are prepared using the extrusion method. The size of vesicles before and after reconstitution is checked using Dynamic Light Scattering (DLS). DLS data confirm an average vesicle diameter of ∼150 nm (SI, Fig. S3). A separated assay for each transmembrane protein respectively further proves their functionality. bR proton pumping and intravesicular acidification interior is detected using pyranine as internal probe (SI, Fig. S4). The activity of ATP synthase is determined in an acid-base transition experiment (SI, Fig. S5). ATP production in the co-reconstituted module under illumination is measured using the luciferin/luciferase assay (Fig. 1B). The achieved maximal rate of 4.5 µmol ATP $(mgEF_OF_1)^{-1}min^{-1}$ is high compared to literature work. An overview of different light-driven and chemically-driven ATP regeneration modules and their ATP production rates can be found in our recent article (1). We mainly attribute this comparably high efficiency of ATP production to the increased amount of bR reconstituted in our system, aiming for a theoretical ratio of 1 ATP synthase and 96 bR molecules per liposome with an almost uniform direction. In most of the literature work (1, 23, 25, 27, 34) significant lower bR concentrations were used for co-reconstitution. Only Racker and Stoeckenius (35) as well as Choi and Montemagno (36) applied bR concentrations of similar magnitude. Moreover, we found out that the vesicle preparation method has significant impact on the performance of the ATP module. Using dialysis liposomes instead of vesicles produced by extrusion method leaded to around 50% decreased activity. Dithiothreitol (DTT) was shown to have a positive effect on the ATP production rates by preventing oxidation and therefore conserving proteins in their functional form. Only 43% of activity was remaining in the absence of

DTT. In contrast to literature reports, we used ultra pure ADP (>99.9%) in our measurements. The commonly offered ADP salt is highly contaminated with ATP, leading to inhibition of ATP synthase by ATP itself. Therefore, significantly higher ATP production rates can be observed using ultra pure ADP solution.

2.1 Light-driven reactivation of flagella

Next, we coupled the light-driven ATP regeneration module with flagella (∼10 μm in length) isolated from green algae *C. reinhardtii* (37), as schematically displayed in Fig. 2A. Upon illumination, ATP is synthesized which powers the activity of axonemal dyneins, converting chemical energy to mechanical work by sliding neighboring microtubule doublets relative to each other. However, due to mechanical constrains, MT doublets are not free to slide, instead sliding will be converted to rhythmic bending deformations that propagate along the contour length of axonemes with a frequency which depends on ATP concentration (supplemental video 1). As shown in Fig. 2B and 2C, higher ATP concentrations are produced by illuminating the energy module for a longer period of time. Interestingly, we observed that even after 1 min of illumination with microscope light, ∼1 µM ATP was produced which was sufficient to reactivate axonemes with a beating frequency of around 20 Hz (see Fig. 3). Our quantitative analysis of beating frequency of reactivated axonemes confirm that they beat faster at higher ATP concentrations produced by longer illumination periods (Fig. 2D). These results are in agreement with the frequency trend reported by Geyer et.al. (38). However, in contrast to Ref. (38), we observed that axonemes beat even at ATP concentrations well below 30 µM. We performed experiments with fluorescently labeled vesicles to examine possibility of vesicle accumulation in the vicinity of axonemes which can locally synthesize higher ATP concentrations upon illumination. These experiments did not confirm any significant higher fluorescent intensity in the areas close to the axonemes.

Figure 3A-B shows exemplary oscillatory motion of an axoneme in response to ATP generated by light-driven energy module pre-illuminated for 45 mins (supplemental video 2). We observed bending deformations propagating with frequency of up to 72 Hz from basal end towards the distal tip (Fig. 3C). To analyze the oscillatory motion of axonemes, we first tracked filaments using gradient vector flow (GVF) technique (39, 40) and quantified the curvature waves (see Figs. 3C, S6 and Materials and Methods). To characterize the mean shape of axonemes which is a static circular arc (the filament in cyan color in Fig. 3D), we translated and rotated configurations of an actively beating axoneme such that the basal end defined as $s = 0$ is at position $(0, 0)$ and the tangent vector at the basal end is orientated in the $\hat{x}$ direction (Fig. 3D). Figure 2D illustrates that curvature of the mean shape of axonemes does not significantly depend on ATP concentration produced upon illumination (38). This static curvature (∼0.2 µm^{-1}) leads to a circular swimming trajectory of axonemes (Fig. 3B) and can be reduced by adding calcium ions to the reactivation buffer (41). Figure 3F-K shows an example that static curvature has been reduced to 0.03 µm^{-1} by adding 1 mM $CaCl_2$ and thereby axoneme swims in a straight trajectory (see video 3). Since the energy module is not pre-illuminated, 1 min illumination by microscope light synthesized ∼1 µM ATP, which was enough to reactivate axonemes at the reduced beating frequency of 20 Hz. We emphasize that beating

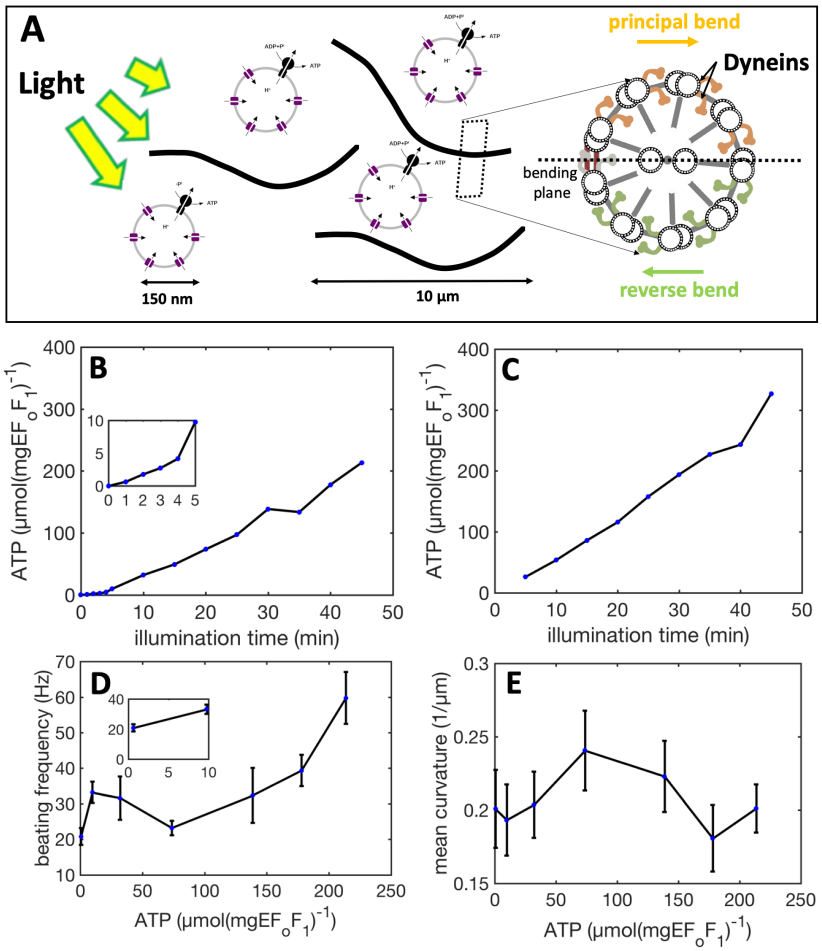

Fig. 2: A) Schematic representation of light-powered energy module integrated with isolated flagella. Functionalized liposomes are illuminated for different times, generating ATP concentrations up to 330 µM. Dyneins in orange and green color bend the axoneme in opposite directions. B) Illumination under microscope light (5W) and C) illumination with a LED lamp (50 W). Both light sources are located 25 cm away from the sample. Inset shows ATP production in the time interval 0 to 5 min of illumination. D) Axonemes beat faster at higher ATP concentrations produced by longer illumination of energy module under microscope light. Inset shows that axonemes beat even at small ATP concentrations. E) Static curvature of the axoneme does not significantly depend on ATP concentration. For each data point in parts D and E, frequencies of 10 axonemes are calculated to obtain the standard deviations.

frequency, static curvature and amplitude of deformation waves are directly coupled to swimming trajectory and a faster beating flagellum with reduced static curvature but the same wave amplitude swims on average a longer distance (see Materials and Methods and Fig. S7 for simulations on swimming trajectory).

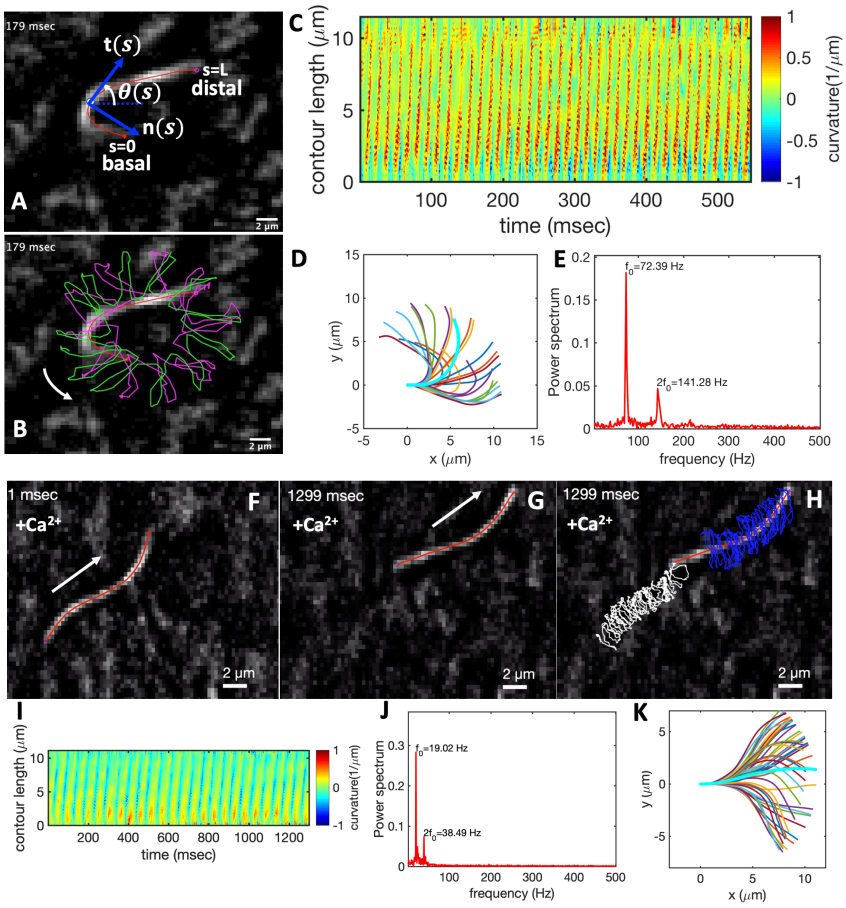

Fig. 3: Reactivation of axonemes by light-driven energy module with different illumination periods. (A) An actively beating axoneme fueled by 213 µM ATP produced upon illumination of energy module for 45 min by microscope light (see video 2). (B) As axoneme beats with frequency of 72 Hz, it rotates CCW with slower frequency of 2 Hz. Magenta and green trajectories show the traces of distal and basal ends of the axoneme, respectively. (C) Curvature waves propagate along the contour length from the basal towards the distal end. (D) Configurations of the axoneme at different time points are translated and rotated such that basal end is at $(0, 0)$ and the orientation of the tangle vector at the basal end is in the $\hat{x}$ direction. Static curvature of axoneme is $\sim 0.2\,\mu\text{m}^{-1}$ (E) Power spectrum showing dominant peaks at $f_0 = 72$ Hz and at second harmonic $2f_0$. F-K) A separate experiment with 1 mM $CaCl_2$ which reduces the static curvature of the axoneme to $0.01\,\mu\text{m}^{-1}$ (compare filaments with cyan color in parts D and K). Thus, the axoneme swims in a more straight trajectory (compare parts B and H) utilizing $\sim$1 µM ATP synthesized by energy of microscope light without 45 min pre-illumination step. At such a low ATP concentration axoneme beats at slower frequency of 19 Hz (see video 3).

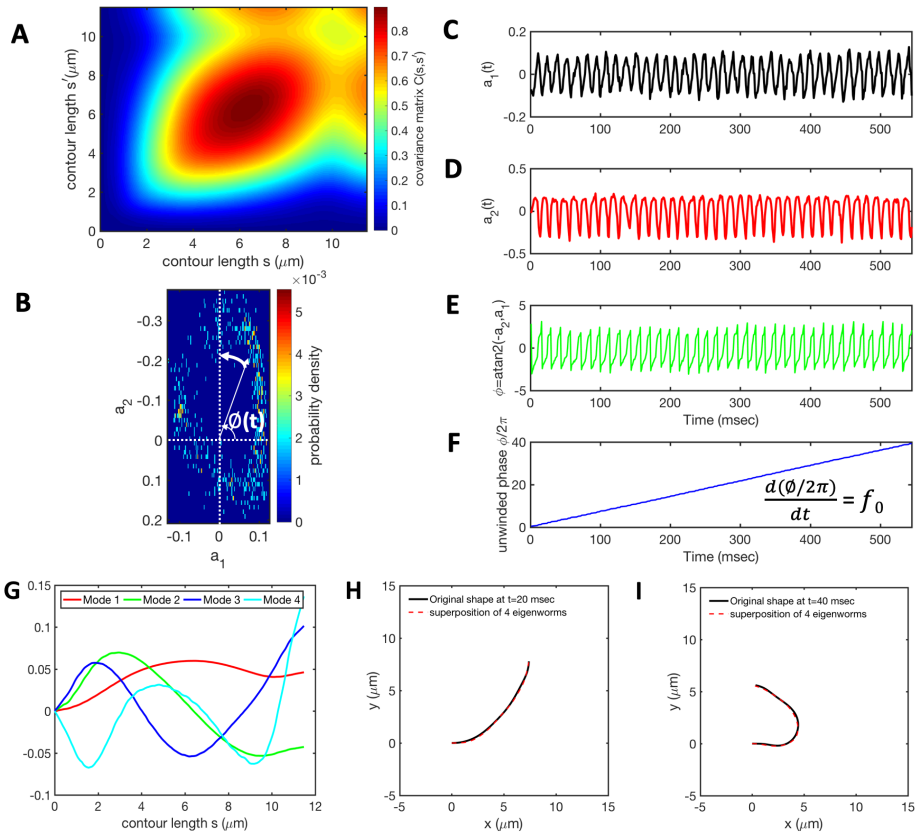

Fig. 4: Mode analysis of the reactivated axoneme presented in Fig. 3A-E. A) The covariance matrix $C(s, s')$ of fluctuations in angle $\theta(s, t)$. B) The probability distribution of the first two shape amplitudes $p(a_1(t), a_2(t))$. The phase angle of the axoneme as an oscillator is defined as $\phi(t) = \text{atan2}(-a_2(t), a_1(t))$. C-D) Time evolution of the first two dominant shape amplitudes $a_1(t)$ and $a_2(t)$ showing regular oscillations at frequency of 72 Hz. E-F) We observe a linear growth in dynamics of $\phi(t)$, indicating steady rotation in $a_1 - a_2$ plane presented in part B. Note that $d\phi/dt = 2\pi f_0$ where f_0 is the beating frequency of axoneme. G) Four eigenvectors corresponding to the four largest eigenvalues of matrix $C(s, s')$. H-I) Superposition of four eigenmodes presented in part G with coefficients $a_1(t)$ to $a_4(t)$, can reproduce shape of the axoneme with high accuracy.

To describe shape dynamics of axonemes, we followed principal mode analysis introduced by Stephens et al. (42) (see Materials and Methods). First, we used data of tracked axonemes obtained by GVF technique (39, 40) to compute $\theta(s, t)$ which is defined as the angle between the local tangent vector and $\hat{x}$ axis (see Fig. 3A). Next, we calculated covariance matrix $C(s, s')$ of fluctuations in angle which has only a small number of nonzero eigenvalues. The color map of this matrix presented in Fig. 4A shows that $C(s, s')$ has an effective reduced dimensionality. As shown by Stephens et al. (42) for C.elegance, only four eigen-

vectors $V_n(s)$ $(n = 1, .., 4)$ corresponding to the first four largest eigenvalues of covariance matrix are enough to describe shape of axoneme with high accuracy (Fig.4G, H and I). The first two motion amplitudes $a_1(t)$ and $a_2(t)$ are shown in Fig. 4C, D and the corresponding probability density is presented in Fig. 4B (see Materials and Methods). Considering reactivated axonemes as an example of a self-sustained biological oscillator, it is possible to define a phase which facilitates quantitative analysis. To present instantaneous state of an oscillator, we consider the stable limit cycle that forms in $a_1 - a_2$ plane, and define phase as a monotonically increasing function $\phi(t)$ (Fig. 4B, F). For a given limit cycle, phase ϕ rotates uniformly in the phase space such that $d\phi/dt = 2\pi f_0$, where f_0 is the autonomous beating frequency of axoneme (Fig. 4F).

2.2 Light-driven contraction of MTs/kinesin-1 network

We tested the suitability of light-switchable energy module for encapsulated *in vitro* motility assays constituted of microtubules and force-generating molecular motors. This assembly under illumination provides an energetically autonomous system that has the potential to advance the development of synthetic cells. We verified the activity of the motor-driven filamentous network by characterizing its activity in water-in-oil droplets with various diameters between 30 and 70 µm.

Figure 5 and supplemental video 4 show the contraction of MTs/kinesin-1 network mixed with the pre-illuminated photosynthetic energy module and encapsulated in a microfluidic device (see Materials and Methods and Fig. S8 for the design of the set up). We observed a uniform distribution of the network immediately after encapsulation, as shown in Fig. 5B. Over time, ATP produced in pre-illuminated energy module drives the activity of molecular motors enabling them to cross-link and slide neighboring MTs against each other which results in a net force that contracts the network. A snapshot of the contracted network after 40 mins is shown in Fig. 5C. We quantified the contractile activity of the system by analyzing the relative reduction in the network area over time. Figure 5D, E show that network contraction inside droplets of different diameters occurs at the similar time-scales.

We note that discontinuous illumination of the sample by microscope light during imaging produces ATP which compensates consumption of ATP by molecular motors. We verified this circulating energy-production and consumption in the system by a separate experiment where we confined MTs/kinesin-1 network in a milli-fludic device with rectangular cross-section (30 mm×1.5 mm×0.1 mm). The aim here is to compare network contractility in areas illuminated by discontinuous microscope light where ATP is consumed and produced, versus non-illuminated areas where ATP is only consumed but not replenished by light. Figure 6 shows that initially the active network fills the entire 3D volume of the channel. Kinesin-1 motors consume ATP synthesized in pre-illuminated energy module, generating active stresses which results in network contraction (Fig. 6B). As kinesin-1 motors consume ATP, discontinuous microscope illumination compensates ATP consumption and motor-driven network contraction reaches its maximum value of 38.6% within 60 min, as displayed in Fig. 6C and supplemental video 5. ATP production is maintained only in areas illuminated by the microscope light, causing stronger network contraction compared to non-illuminated regions in the channel. We observed reduced contractility of around 10% in the adjacent volume near the region il-

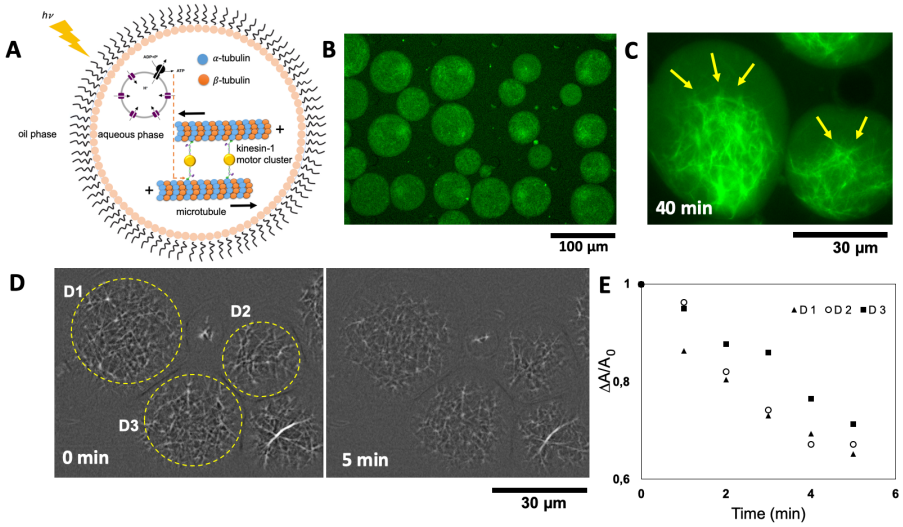

Fig. 5: A) Schematic presentation of MTs/kinesin1 network encapsulated in water-in-oil droplets. Upon illumination, synthetic vesicles synthesize ATP, providing fuel for kinesin-1 clusters which are plus-end directed motors and slide MTs relative to each other. B) MTs/kinesin-1 network show a uniform distribution shortly after encapsulation. The droplet size varies between 30 to 70 µm. C) Snapshots of network contraction after 40 mins. The yellow arrows highlight the network contraction. D) Snapshots of contractile active network at two different time points. The yellow circles mark the area covered by the network at $t = 0$. E) Relative reduction of network area over time for three droplets of different diameters (26, 31, 43 µm). A_0 is the initial area of the network before contraction.

luminated by the microscope light, as shown in Figure 6D. These experiments suggest that by applying a patterned-illumination in a filamentous network, different contraction-maps with spatial gradient can be imposed. Further, it demonstrates the efficiency of the light-driven energy module for controlled and localized ATP production and underline the potential application of this system in the field of synthetic biology with the ultimate goal of building an artificial cell.

3 Discussion

Our experiments demonstrate that light-switchable photosynthetic liposomes can drive ATP-dependent activity of axonemal dyneins which serve as tiny protein machinery converting chemical energy into mechanical work in the form of a rhythmic beating pattern. We used energy of light for dynamic synthesis of ATP, allowing us to control beating frequency of axonemes as a function of illumination. We note that static and dynamic components of curvature waves combined with beating frequency determine the swimming trajectory of isolated flagella. In the context of targeted drug delivery, light-powered flagella attached

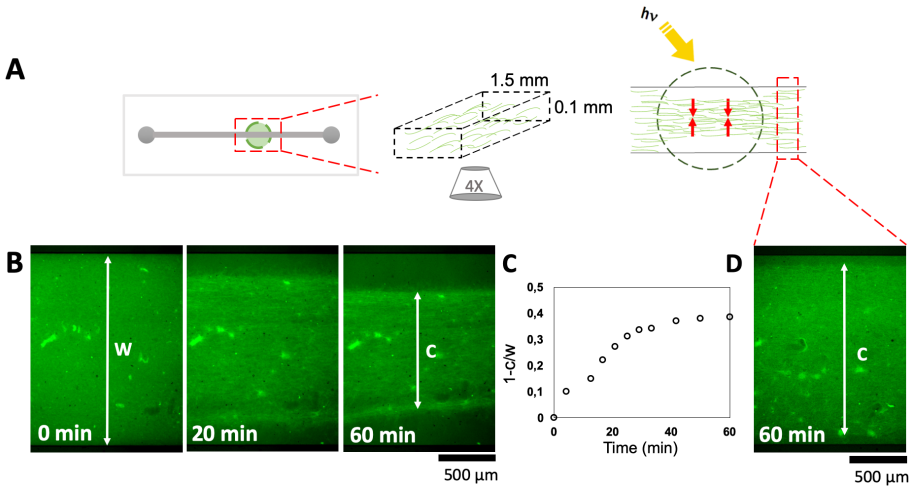

Fig. 6: Photo-stimulated contraction of MTs/kinesin-1 network in a milli-fluidic device. A) Schematic representation of the milli-fluidic device highlighting the area which is illuminated by discontinuous microscope light. Taxol-stabilized MTs are mixed with kinesin-1 motors and pre-illuminated energy module before injection into a milli-fluidic channel. B) Over time, existing ATP in the pre-illuminated energy module is consumed by force-generating kinesin-1 motors. Microscope illumination compensates for ATP consumption and filamentous network contracts up to 38%. C) Quantitative analysis of the network contraction in illuminated region shows a linear increase at the first 40 mins, reaching a plateau after 60 mins. D) In the non-illuminated areas where ATP is being consumed but not replenished, we observe a reduced contractility of 10% after 1 hour.

to drug-loaded vesicles from one end and magnetic beads from other end form a complex which may have potential biomedical applications in controlled delivery and release of drugs. While the flagella provides propulsion upon illumination, magnetic beads driven by external magnetic field can be used for guidance and release of the flagella-drug complex (43).

Furthermore, we have shown that functionalized artificial liposomes, capable of continuous production of ATP by shining light as external stimulus, can serve as an efficient energy module for *in vitro* microtubule motility assays where kinesin-1 molecular motors are actively engaged in generating and sustaining active stresses in the network. Our developed scheme with circulating energy consumption and production could serve as a potential platform to encapsulate constituent elements such as actin, microtubules and various regulatory components inside functionalized lipid vesicles, providing ATP in an optical-controllable self-sustained fashion. ATP-driven motor activity in filamentous biopolymer networks is expected to generate active forces, driving morphological deformations in liposomes, and will further contribute to achieving the challenging goal of designing an artificial cell from the bottom-up approach.

4 Material and Methods

4.1 Expression and purification of membrane proteins

Purple membrane was isolated from Halobacterium salinarium (strain S9) as described by Oesterhelt (32). His-tagged E. coli F_OF_1-ATP synthase (EF_OF_1) was expressed from the plasmid pBWU13-βHis in the E. coli strain DK8 (ΔuncBEFHAGDC) and purified by Ni-NTA affinity chromatography as previously described by Ishmukhametov, Galkin, and Vik (31)

4.2 Preparation of lipid vesicles for light-driven ATP production

Vesicles were formed by film rehydration method followed by extrusion. 10 mg of dissolved phosphatidylcholine lipid was deposited in a glass vial and solvent was removed using a gentle stream of nitrogen. Thin lipid films were rehydrated in HMDEKP buffer (30 mM HEPES-KOH, 5 mM $MgSO_4$, 1 mM DTT, 1 mM EGTA, 50 mM potassium acetate, 1 % PEG, pH 7.4) to a final concentration of 10 mg/ml by vortexing. To transform multilamellar vesicles into unilamellar vesicles, the suspension was subjected to 5 freeze-thaw cycles. Each cycle consisted of freezing in liquid nitrogen, thawing in a 35°C water bath and vortexing for 30 s. Suspensions were extruded 11 times through a 100 nm pore size polycarbonate membrane (Whatman) to form uniform vesicles.

4.3 Co-reconstitution of EF_OF_1-ATP synthase and bR

100 µL of preformed vesicles were mixed with 0.1 µM EF_OF_1-ATP synthase and 9.9 µM bR in form of membrane patches. 0.8 % Triton X-100 was added under vortexing to partially solubilize the vesicles. After 15 minutes incubation in the dark under gentle shaking, 80 mg of wet SM-2 Bio-Beads were added and the solution was incubated for further 60 minutes under constant shaking in the dark.

4.4 Light-induced ATP production

For measurement of light-induced ATP production, 25 µL of co-reconstituted vesicles were diluted in 250 µL of HMDEK buffer (30 mM HEPES-KOH, 5 mM $MgSO_4$, 1 mM DTT, 1 mM EGTA, 50 mM potassium acetate, pH 7.4) supplemented with 1% (w/v) polyethylene glycol ($M_w = 20\,\mathrm{kg\,mol^{-1}}$) and 1.6 mM ultra pure ADP (Cell Technologies). The reaction was started by illumination with a 50 W green LED lamp or a 5 W microscope light. Aliquots of 25 µL were taken at the beginning every 1 minutes and later on every 5 minutes from the reaction mixtures and the reaction was stopped by addition of the same volume of trichloroacetic acid (40 g/L). The ATP concentration was measured with the luciferin/luciferase assay and calibrated by addition of 10 µL ATP (7.8 µM) after each measurement.

4.5 Isolation and reactivation of flagella with light-driven energy module

Axonemes were isolated from wild-type *Chlamydomonas reinhardtii* cells, strain SAG 11-32b. They were grown axenically in TAP (tris-acetate-phosphate) medium on a 12 h/12 h day-night cycle. Flagella were isolated using dibucaine,(44, 45) then purified on a 25% sucrose cushion, and demembranated using detergent NP-40 in HMDEK solution supplemented with 0.2 mM Pefabloc. The membrane-free axonemes were resuspended in HMDEK buffer plus 1% (w/v) polyethylene glycol ($M_w = 20\,\mathrm{kg\,mol^{-1}}$), 0.2 mM Pefabloc, 20% sucrose and stored at −80 °C. To perform reactivation experiments, we thawed axonemes at room temperature and kept them on ice and used them for up to 2 hours. Next, we diluted axonemes in HMDEKP reactivation buffer (HMDEK plus 1 % PEG) which contains light-driven energy module and is supplemented with 0.2 mM Pefabloc. We infuse them into 100 µm deep flow chambers, built from cleaned glass and double-sided tape. For experiments with calcium, 1 mM $CaCl_2$ was added to HMDEKP reactivation buffer.

4.6 Axoneme contour tracking

We imaged reactivated axonemes using phase-contrast microscopy (100X objective, imaging frequency of 1000 fps). To increase the signal to noise ratio, we first inverted phase-contrast images and then subtracted the mean-intensity of the time series. This background-subtraction method increased the signal to noise ratio by a factor of three (38). Next, we applied a Gaussian filter to smooth the images. Tracking of axonemes is done using gradient vector flow (GVF) technique (39, 40). For the first frame, we select a region of interest that should contain only one actively beating axoneme. Then, we initialize the snake by drawing a line polygon along the contour of the axoneme in the first frame (see Fig. S6). This polygon is interpolated at N equally spaced points and used as a starting parameter for the snake. The GVF is calculated using the GVF regularization coefficient $\mu = 0.1$ with 20 iterations. The snake is then deformed according to the GVF where we have adapted the original algorithm by Xu and Prince for open boundary conditions. We obtain positions of N points along the contour length s of the filament so that $s = 0$ is the basal end and $s = L$ is the distal side, where L is the total contour length of filament. The position of filament at s_i is denoted by $r(s_i) = (x(s_i), y(s_i))$.

4.7 Simulations with simplified wave form

To investigate the influence of frequency, static curvature and amplitude of the curvature waves on swimming trajectory of axoneme, we performed simulations with a simplified form of curvature waves which is a superposition of a dynamic mode (cosine wave) and a static mode (a circular arc) (37):

$$C(s,t) = C_0 + C_1 \cos(2\pi(s/\lambda - f_0 t)), \tag{1}$$

where C_0 is the static curvature, C_1 is the amplitude of the dynamic mode, λ is the wavelength and f_0 is the beating frequency. Minus sign in term $-f_0$ generates waves that propagate from $s = 0$ (basal end) to $s = L$ (distal tip).

As shown in Fig. S7A-B, in the absence of a static curvature ($C_0 = 0$), flagella swims on a straight path and faster beating flagella swims a longer distance. For a non-zero static curvature ($C_0 \neq 0$), which is the case for isolated axonemes in our experiments, flagella swims on a circular path, as shown in Fig. S7C. Note that in our experiments, adding calcium reduces the static curvature C_0 in a dose dependent manner, approaching to almost zero at 1 mM $CaCl_2$ concentration (see Fig. 3K).

In these simulations, we compute drag force density felt by each flagellum in the framework of resistive-force theory (46). In this theory, each flagellum is divided to small cylindrical segments moving with velocity $\mathbf{u}_\perp$ and $\mathbf{u}_\parallel$ in the body-frame and propulsive force is proportional to the local centerline velocity components of each segment in parallel and perpendicular directions.

4.8 Mode analysis

We used the Frenet equations to analyze axoneme's shapes in a plane (42):

$$\frac{d\mathbf{r}(s)}{ds} = \hat{\mathbf{t}}(s) \qquad \text{and} \qquad \frac{d\hat{\mathbf{t}}(s)}{ds} = \kappa(s)\hat{\mathbf{n}}(s). \tag{2}$$

Here $\hat{\mathbf{t}}(s)$ is the unit tangent vector to the axoneme, $\hat{\mathbf{n}}(s)$ is the unit normal vector and $\kappa(s)$ is the curvature (see Fig. 3A). We define $\theta(s)$ to be the angle between the tangent vector at contour length s and the x-axis, then $\kappa(s) = d\theta(s)/ds$. Note that we rotate and translate the axoneme such that point $s = 0$ (basal end) is at position $(x, y) = (0, 0)$ and the local tangent vector at $s = 0$ is in the $\hat{x}$ direction, giving $\theta(0) = 0$. Following Stephens et al.(42), we performed principal mode analysis by calculating the covariance matrix of angles $\theta(s)$ defined as $C(s, s') = \langle(\theta(s) - \langle\theta\rangle)(\theta(s') - \langle\theta\rangle)\rangle$. We then calculated the eigenvalues λ_n and the corresponding eigenvectors $V_n(s)$ of this matrix, showing that superposition of 4 eigenvectors corresponding to four largest eigenvalues can describe the axoneme's shape with high accuracy,

$$\theta(s, t) \approx \sum_{n=1}^{4} a_n(t) V_n(s). \tag{3}$$

Here the four variables $a_1(t), .., a_4(t)$ are the amplitudes of motion along different principal components and are given by $a_n(t) = \sum_s V_n(s)\theta(s)$.

4.9 Motile bundle solution

The motile bundle solution was obtained by mixing taxol-stabilized microtubules and an active mixture (AM) containing molecular motors kinesin-1 clustered in multimotors configuration by using streptavidin. Kinesin 401 was purified as previously published (47, 48) and the kinesin-streptavidin complexes were prepared by mixing 0.2 mg/ml kinesin 401, 0.9 mM dithiothreitol (DTT), 0.1 mg/ml streptavidin dissolved in M2B (80 mM PIPES, adjusted to pH = 6.9 with KOH, 1 mM EGTA, 2 mM $MgCl_2$) and incubated on ice for 15 min.
The AM was obtained by mixing 2.4 mM Trolox, 16.6 µL 3% PEG, 5.5 µL M2B, 3.25 µL DTT (10 mM), the oxygen scavenger (0.2 mg/ml glucose oxidase (Sigma G2133), 0.05 mg/ml catalase (Sigma C40)), 0.5 mg/ml glucose , and 4 µL

kinesin1-streptavidin clusters. The microtubule polymerization mixture (MT) was prepared by mixing 27 µM porcine brain tubulin (1:5 labeled tubulin) in M2B with 5 mM $MgCl_2$, 1 mM GTP, 50 % DMSO and 0.3% PEG. This solution is kept in the oven for 30 minutes by 37°C and diluted up to 200 µL with M2B and 7 µM taxol. The final mixture was prepared by mixing polymerized MT, AM and light-driven ATP module in different amounts depending on the experimental set up.

4.10 Encapsulation of MTs/kinesin-1 network assembled with photosynthetic vesicles

The feasibility of the proposed concept, towards building artificial cells, was demonstrated by encapsulation (water-in-oil droplets, w/o) of MTs/kinesin-1 mixed with pre-illuminated ATP module by droplet microfluidic technique (see Sec. 4.11). Sample containing the MTs/kinesin-1 and 45 min pre-illuminated ATP module with volume ratio of 1:20 v/v (ATP module:MTs mixture) was pumped into inner- inlets (aqueous phase 1 and 2), while oil phase (FluoSurf 2% in HFE 7500 or FC40) was pumped into outer-inlet. Micro syringe pumps (CETONI BASE 120 with neMESYS pumps, Germany) and glass syringes (Hamilton, USA) were used to inject the aqueous and oil phases. Aqueous phases merged with oil phase at T-junction and generated droplets in a continuous mode of device operation (SI, Fig. S8A). Solution of MTs/kinesin-1 and ATP module encapsulated continuously inside water-in-oil droplets at T-junction in a stabilized manner (SI, Fig. S8B) and passed from red to green area of the channel where the height of the micro-channel is reduced to 17 µm to flatten the droplets which helps in microscopy (SI, Fig. S8C). Further, droplets were entrapped between pillars in observation chamber by applying the pressure at top layer which aided in blocking the forward flow (SI, Fig. S8D). Inside observation chamber entrapped-encapsulated MTs/kinesin-1/ATP module were imaged by epi-fluorescence microscope to observe contraction of filamentous network. The size of droplets was measured to be 50 ± 20 µm in diameter.

4.11 Fabrication of the microfluidic device

A schematic presentation of the microfluidic device is shown in Fig. S8A. Polydimethylsiloxane (PDMS) microchannel was fabricated using conventional soft lithography. A thin layer of SU-8 3010 photoresists (MicroChem, Newton, MA) was spin-coated onto a Si wafer and patterned via ultraviolet exposure through a chrome mask. The device has two different heights (red and green parts in Fig. S8A), thereby spin-coating is done in two steps. To fabricate the device, PDMS and the curing agent (SYLGARD 184 Silicone Elastomer) were thoroughly mixed with 10:1 and poured onto the patterned SU-8 mold, followed by degassing to remove bubbles from the PDMS under vacuum pressure. After removing the bubbles and baking at 75°C for 45 min, PDMS was peeled off from the Si substrate, and the microchannels were cut to the appropriate sizes. After punching the inlet and outlet ports, PDMS microchannel was oxygen plasma-bonded (PDC 002, Harrick Plasma, Ithaca, USA) to the glass slide (24 mm×60 mm, Menzel gläser, Germany) for 30s at 200 W and 200 mTorr. To strengthen the bonding, the device was heated in a 75°C oven for at least 2 min. The height of the observation chamber is 13 µm, respectively, whereas the

width was 120 µm. Diameter of pillars and pillar to pillar distance inside observation chamber was 30 and 150 µm, respectively. Micro-channel was coated with Novec^{TM} 1720, 3M at 120 °C for 1 hr to make it hydrophobic.

5 Acknowledgment

R.A., V. N., E. B., I. G. and A. G. acknowledge support from the European Union's Horizon 2020 research and innovation programme under grant agreement MAMI No. 766007. C.K., A.B., E.B., K.S., I.G., T.V.K., and A.G. thank MaxSynBio Consortium, which is jointly funded by the Federal Ministry of Education and Research of Germany and the Max Planck Society. A. G. and R. A. thank M. Lorenz and the Göttingen Algae Culture Collection (SAG) for providing the *Chlamydomonas reinhardtii* strain 11-32b.

Author contributions: A.G. and T.V.K. designed the project. R.A. and A.G. isolated flagella and C.K., and T.V.K. built the energy module. R.A. and C.K. integrated the energy and flagella motility unit. R. A., V. N. and I. G. performed experiments with MT networks. R.A., C.K., Y.S., S.G.P. and A.G. analyzed the data. A. G. performed the mode analysis of axonemes and A.B. wrote the Matlab code to track the axonemes. All the authors discussed the results and R.A., C.K., V. N., I. G., T.V.K. and A.G. wrote the manuscript.

Competing interests: The authors declare that they have no competing financial interests.

References

(1) L. Otrin, C. Kleineberg, L. Caire da Silva, K. Landfester, I. Ivanov, M. Wang, C. Bednarz, K. Sundmacher, and T. Vidaković-Koch. "Artificial organelles for energy regeneration". In: *Advanced Biosystems* 3.6 (2019), p. 1800323.

(2) K. Göpfrich, I. Platzman, and J. P. Spatz. "Mastering complexity: towards bottom-up construction of multifunctional eukaryotic synthetic cells". In: *Trends in biotechnology* 36.9 (2018), pp. 938–951.

(3) P. Schwille, J. Spatz, K. Landfester, E. Bodenschatz, S. Herminghaus, V. Sourjik, T. J. Erb, P. Bastiaens, R. Lipowsky, A. Hyman, et al. "MaxSynBio: avenues towards creating cells from the bottom up". In: *Angewandte Chemie International Edition* 57.41 (2018), pp. 13382–13392.

(4) D. Fletcher. *Which biological systems should be engineered?* 2018.

(5) D. Pantaloni, C. Le Clainche, and M.-F. Carlier. "Mechanism of actin-based motility". In: *Science* 292.5521 (2001), pp. 1502–1506.

(6) T. D. Pollard and G. G. Borisy. "Cellular motility driven by assembly and disassembly of actin filaments". In: *Cell* 112.4 (2003), pp. 453–465.

(7) J. R. Blake and M. A. Sleigh. "Mechanics of ciliary locomotion". In: *Biological Reviews* 49.1 (1974), pp. 85–125.

(8) T. Ishikawa. "Axoneme structure from motile cilia". In: *Cold Spring Harbor perspectives in biology* 9.1 (2017), a028076.

(9) Z. Carvalho-Santos, J. Azimzadeh, J. B. Pereira-Leal, and M. Bettencourt-Dias. "Tracing the origins of centrioles, cilia, and flagella". In: *J Cell Biol* 194.2 (2011), pp. 165–175.

(10) P. Satir and S. T. Christensen. "Overview of structure and function of mammalian cilia". In: *Annu. Rev. Physiol.* 69 (2007), pp. 377–400.

(11) D. Nicastro, C. Schwartz, J. Pierson, R. Gaudette, M. E. Porter, and J. R. McIntosh. "The molecular architecture of axonemes revealed by cryoelectron tomography". In: *Science* 313.5789 (2006), pp. 944–948.

(12) G. J. Pazour, N. Agrin, J. Leszyk, and G. B. Witman. "Proteomic analysis of a eukaryotic cilium". In: *The Journal of cell biology* 170.1 (2005), pp. 103–113.

(13) T. Yagi, K. Uematsu, Z. Liu, and R. Kamiya. "Identification of dyneins that localize exclusively to the proximal portion of Chlamydomonas flagella". In: *Journal of cell science* 122.9 (2009), pp. 1306–1314.

(14) I. Milisav. "Dynein and dynein-related genes". In: *Cell motility and the cytoskeleton* 39.4 (1998), pp. 261–272.

(15) I. Gibbons. "Studies on the adenosine triphosphatase activity of 14 S and 30 S dynein from cilia of Tetrahymena". In: *Journal of Biological Chemistry* 241.23 (1966), pp. 5590–5596.

(16) K. Ogawa and H. Mohri. "Studies on flagellar ATPase from sea urchin spermatozoa. I. Purification and some properties of the enzyme". In: *Biochimica et Biophysica Acta (BBA)-Bioenergetics* 256.1 (1972), pp. 142–155.

(17) J. Lin, D. Tritschler, K. Song, C. F. Barber, J. S. Cobb, M. E. Porter, and D. Nicastro. "Building blocks of the nexin-dynein regulatory complex in Chlamydomonas flagella". In: *Journal of Biological Chemistry* 286.33 (2011), pp. 29175–29191.

(18) T. D. Pollard, W. C. Earnshaw, J. Lippincott-Schwartz, and G. Johnson. *Cell Biology E-Book*. Elsevier Health Sciences, 2016.

(19) P. Dustin. *Microtubules*. Springer Science & Business Media, 2012.

(20) Y. Bashirzadeh and A. P. Liu. "Encapsulation of the cytoskeleton: towards mimicking the mechanics of a cell". In: *Soft Matter* 15.42 (2019), pp. 8425–8436.

(21) L. Otrin, N. Marui, C. Bednarz, T. Vidakovic-Koch, I. Lieberwirth, K. Landfester, and K. Sundmacher. "Toward artificial mitochondrion: mimicking oxidative phosphorylation in polymer and hybrid membranes". In: *Nano letters* 17.11 (2017), pp. 6816–6821.

(22) C. Kleineberg, C. Wölfer, A. Abbasnia, D. Pischel, C. Bednarz, I. Ivanov, T. Heitkamp, M. Börsch, K. Sundmacher, and T. Vidakovic-Koch. "Light-driven ATP regeneration in diblock/grafted hybrid vesicles". In: *ChemBioChem* (2020).

(23) G. Steinberg-Yfrach, J.-L. Rigaud, E. N. Durantini, A. L. Moore, D. Gust, and T. A. Moore. "Light-driven production of ATP catalysed by F 0 F 1-ATP synthase in an artificial photosynthetic membrane". In: *Nature* 392.6675 (1998), pp. 479–482.

(24) J.-L. Rigaud, B. Pitard, and D. Levy. "Reconstitution of membrane proteins into liposomes: application to energy-transducing membrane proteins". In: *Biochimica et Biophysica Acta (BBA)-Bioenergetics* 1231.3 (1995), pp. 223–246.

(25) S. Matuschka, K. Zwicker, T. Nawroth, and G. Zimmer. "ATP synthesis by purified ATP-synthase from beef heart mitochondria after coreconstitution with bacteriorhodopsin". In: *Archives of biochemistry and biophysics* 322.1 (1995), pp. 135–142.

(26) P. Richard and P. Gräber. "Kinetics of ATP synthesis catalyzed by the H+-ATPase from chloroplasts (CF0F1) reconstituted into liposomes and coreconstituted with bacteriorhodopsin". In: *European journal of biochemistry* 210.1 (1992), pp. 287–291.

(27) B. Pitard, P. Richard, M. Duñach, and J.-L. Rigaud. "ATP synthesis by the F0F1 ATP synthase from thermophilic Bacillus PS3 reconstituted into liposomes with bacteriorhodopsin: 2. Relationships between proton motive force and ATP synthesis". In: *European journal of biochemistry* 235.3 (1996), pp. 779–788.

(28) T. E. Miller, T. Beneyton, T. Schwander, C. Diehl, M. Girault, R. McLean, T. Chotel, P. Claus, N. S. Cortina, J.-C. Baret, et al. "Light-powered CO2 fixation in a chloroplast mimic with natural and synthetic parts". In: *Science* 368.6491 (2020), pp. 649–654.

(29) K. Y. Lee, S.-J. Park, K. A. Lee, S.-H. Kim, H. Kim, Y. Meroz, L Mahadevan, K.-H. Jung, T. K. Ahn, K. K. Parker, et al. "Photosynthetic artificial organelles sustain and control ATP-dependent reactions in a protocellular system". In: *Nature biotechnology* 36.6 (2018), pp. 530–535.

(30) S. Berhanu, T. Ueda, and Y. Kuruma. "Artificial photosynthetic cell producing energy for protein synthesis". In: *Nature communications* 10.1 (2019), pp. 1–10.

(31) R. R. Ishmukhametov, M. A. Galkin, and S. B. Vik. "Ultrafast purification and reconstitution of His-tagged cysteine-less Escherichia coli F1Fo ATP synthase". In: *Biochimica Et Biophysica Acta (BBA)-Bioenergetics* 1706.1-2 (2005), pp. 110–116.

(32) D. Oesterhelt. "Isolation of the cell membrane of Halobacterium halobium and its fractionation into red and purple membrane". In: *Methods Enzymol.* 31 (1974), pp. 667–678.

(33) S. Fischer and P. Gräber. "Comparison of ΔpH-and Δφ-driven ATP synthesis catalyzed by the H+-ATPases from Escherichia coli or chloroplasts reconstituted into liposomes". In: *FEBS letters* 457.3 (1999), pp. 327–332.

(34) N. WAGNER, M. GUTWEILER, R. PABST, and K. DOSE. "Coreconstitution of bacterial ATP synthase with monomeric bacteriorhodopsin into liposomes: A comparison between the efficiency of monomeric bacteriorhodopsin and purple membrane patches in coreconstitution experiments". In: *European journal of biochemistry* 165.1 (1987), pp. 177–183.

(35) E. Racker and W. Stoeckenius. "Reconstitution of purple membrane vesicles catalyzing light-driven proton uptake and adenosine triphosphate formation". In: *Journal of Biological Chemistry* 249.2 (1974), pp. 662–663.

(36) H.-J. Choi and C. D. Montemagno. "Artificial organelle: ATP synthesis from cellular mimetic polymersomes". In: *Nano letters* 5.12 (2005), pp. 2538–2542.

(37) V. F. Geyer, P. Sartori, B. M. Friedrich, F. Jülicher, and J. Howard. "Independent control of the static and dynamic components of the Chlamydomonas flagellar beat". In: *Current Biology* 26.8 (2016), pp. 1098–1103.

(38) V. Geyer. "Characterization of the flagellar beat of the single cell green alga *Chlamydomonas reinhardtii*". PhD thesis. Sächsische Landesbibliothek-Staats-und Universitätsbibliothek Dresden, 2013.

(39) C. Xu and J. L. Prince. "Gradient vector flow: A new external force for snakes". In: *IEEE Proc. CVPR*. IEEE. July 1997, pp. 66–71. ISBN: 0-8186-7822-4. DOI: 10.1109/CVPR.1997.609299.

(40) C. Xu and J. L. Prince. "Snakes, shapes, and gradient vector flow". In: *IEEE Transactions on image processing* 7.3 (1998), pp. 359–369.

(41) J. A. Schmidt and R. Eckert. "Calcium couples flagellar reversal to photostimulation in Chlamydomonas reinhardtii". In: *Nature* 262.5570 (1976), pp. 713–715.

(42) G. J. Stephens, B. Johnson-Kerner, W. Bialek, and W. S. Ryu. "Dimensionality and dynamics in the behavior of C. elegans". In: *PLoS computational biology* 4.4 (2008).

(43) H. Xu, M. Medina-Sánchez, V. Magdanz, L. Schwarz, F. Hebenstreit, and O. G. Schmidt. "Sperm-hybrid micromotor for targeted drug delivery". In: *ACS nano* 12.1 (2018), pp. 327–337.

(44) G. B. Witman. "Isolation of Chlamydomonas flagella and flagellar axonemes". In: *Meth. Enzymology*. Vol. 134. Elsevier, 1986, pp. 280–290.

(45) J. Alper, V. Geyer, V. Mukundan, and J. Howard. "Reconstitution of flagellar sliding". In: *Meth. Enzymology*. Vol. 524. Elsevier, 2013, pp. 343–369.

(46) J. Gray and G. Hancock. "The propulsion of sea-urchin spermatozoa". In: *Journal of Experimental Biology* 32.4 (1955), pp. 802–814.

(47) S. P. Gilbert and K. A. Johnson. "Expression, purification, and characterization of the Drosophila kinesin motor domain produced in Escherichia coli". In: *Biochemistry* 32.17 (1993), pp. 4677–4684.

(48) E. C. Young, E. Berliner, H. K. Mahtani, B. Perez-Ramirez, and J. Gelles. "Subunit interactions in dimeric kinesin heavy chain derivatives that lack the kinesin rod". In: *Journal of Biological Chemistry* 270.8 (1995), pp. 3926–3931.

6 Supplementary Information

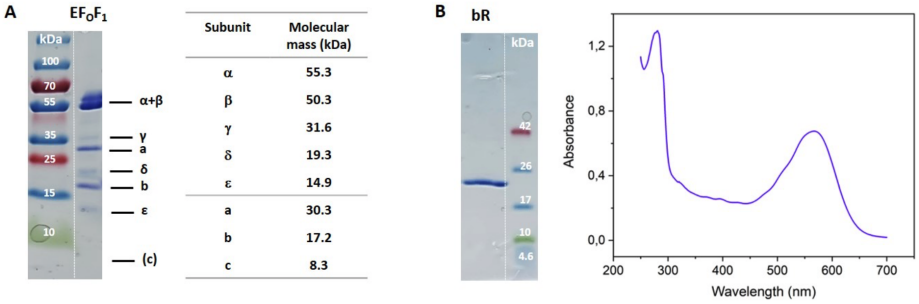

Subunit	Molecular mass (kDa)
α	55.3
β	50.3
γ	31.6
δ	19.3
ε	14.9
a	30.3
b	17.2
c	8.3

Fig. S1: SDS-PAGE of purified proteins. (A) Coomassie-stained SDS-PAGE of purified EF$_O$F$_1$-ATP synthase and molecular masses of EF$_O$F$_1$ subunits. (B) Coomassie-stained SDS-PAGE of purified bR with the corresponding absorbance spectrum.

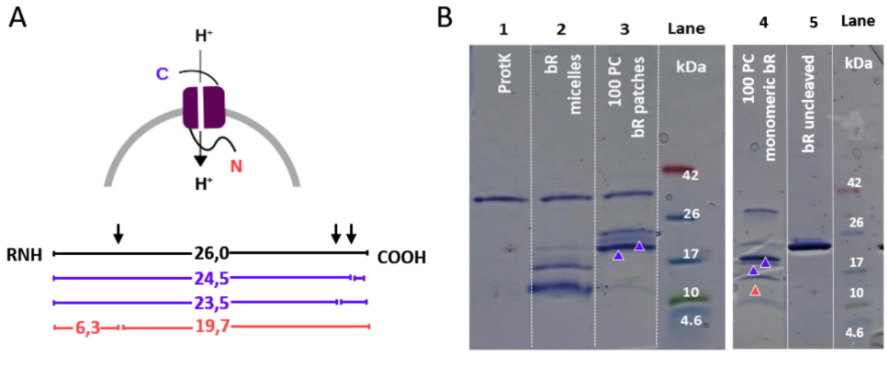

Fig. S2: Proteolytic cleavage of reconstituted bR with proteinase K (ProtK) shows mixed orientation for monomeric bR and almost uniform orientation (with the c terminus outwards) for bR patches. (A) Expected sizes of proteolytic fragments for ProtK digestion of bR when the N-terminal (orange values) or C-terminal (violet values) is exposed to the bulk solution (B) SDS PAGE gel analysis of the digestion products. Lane 1: band specific for ProtK enzyme only; lane 2: digestion product of not reconstituted bR; lane 3: digest pattern for PC vesicles containing bR patches; lane 4: digest pattern for PC vesicles containing monomeric bR; lane 5: undigested bR in PC lipid vesicles.

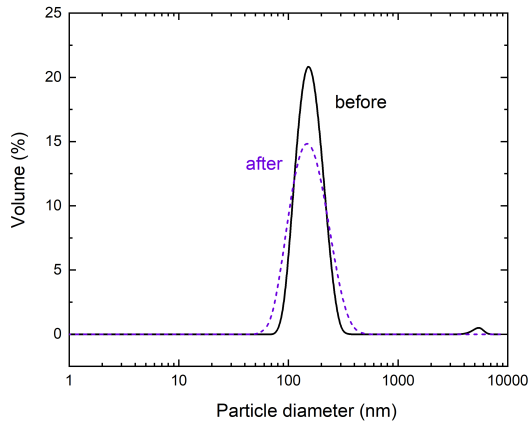

Fig. S3: Size distribution of vesicles before (before) and after reconstitution and removal of detergent using Bio Beads (after).

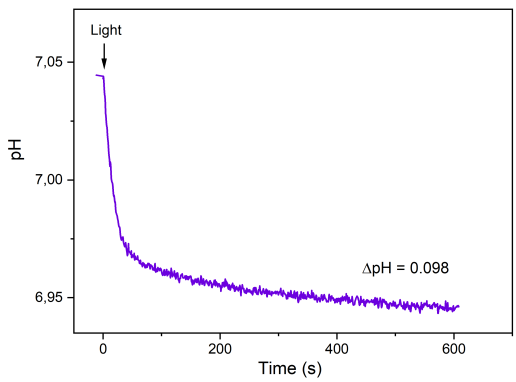

Fig. S4: Proton pumping of bR as measured by encapsulated pyranine.

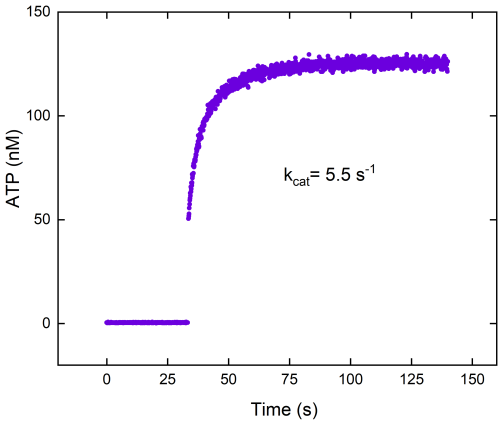

Fig. S5: Turnover (k_{cat}) of ATP synthase as determined in an acid-base transition experiment.

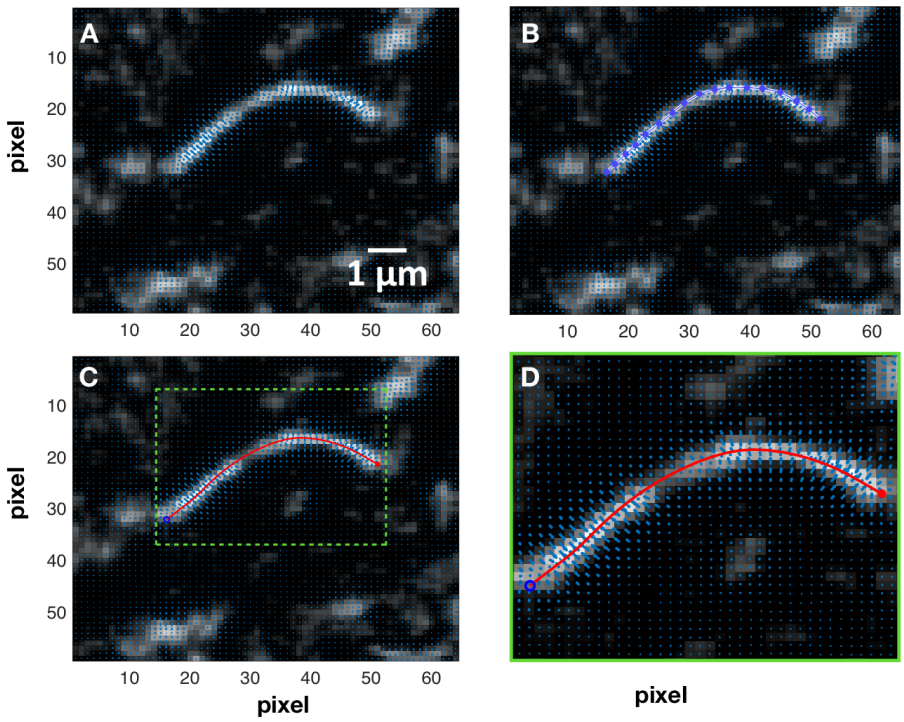

Fig. S6: A) Gradient vector flow calculated at the vicinity of an axoneme. B) The initial selection of a polygon for the first frame which deforms according to the gradient vector flow. C) The final tracked shape of an axoneme. D) A zoomed-in image showing the gradient vector flow (blue arrows) at a higher magnification.

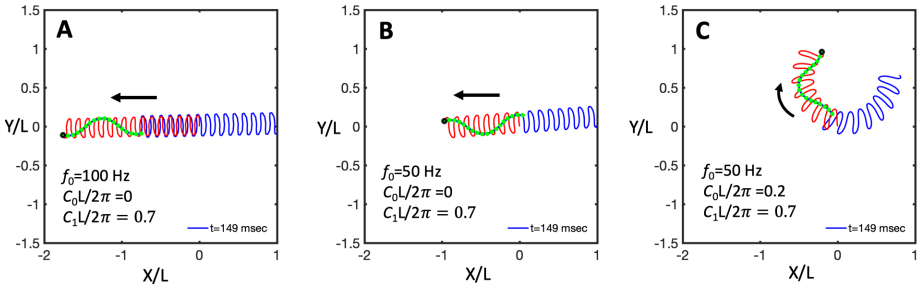

Fig. S7: A-B) A flagellum swimming in the absence of static curvature C_0 at two different frequencies of 100 and 50 Hz. Faster beating flagellum swims a longer distance. C) Flagellum follows a circular path if C_0 is non-zero. Amplitude of the dynamic mode C_1 is kept the same for all three simulations. L is the contour length of flagellum.

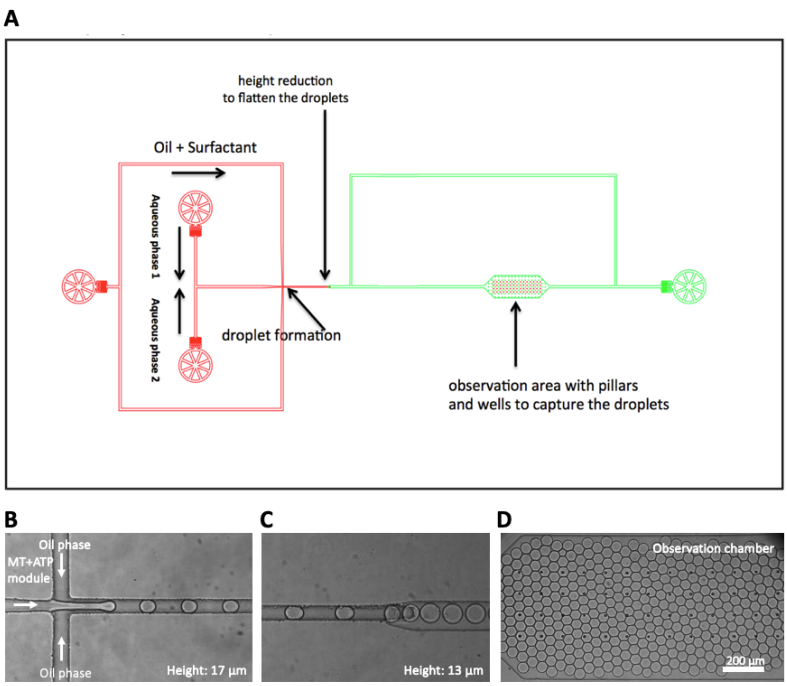

Fig. S8: Droplet microfluidic setup. A) Schematic diagram showing the encapsulation of MTs/kinesin-1 network (aqueous phase 1) with light-driven ATP module (aqueous phase 2). B) Droplet formation at T-junction contained MTs/kinesin-1 with light-driven ATP module (water-in-oil droplets, W/O). C) Droplets enter the green area where height is decreased from 17 to 13 µm. D) Observation chamber with entrapped droplets where the flow into the chamber was stopped by guiding the flow to the side channel. The following flow rates were adjusted: aqueous phase 1, 200 μL/h; aqueous phase 2, 200 μL/h; oil phase, 400 μL/h.